

Harnessing nuclear spin polarization fluctuations in a semiconductor nanowire

P. Peddibhotla¹, F. Xue¹, H. I. T. Hauge², S. Assali², E. P. A. M. Bakkers^{2,3} and M. Poggio^{1*}

Soon after the first measurements of nuclear magnetic resonance in a condensed-matter system, Bloch¹ predicted the presence of statistical fluctuations proportional to $1/\sqrt{N}$ in the polarization of an ensemble of N spins. Such spin noise² has recently emerged as a critical ingredient for nanometre-scale magnetic resonance imaging^{3–6}. This prominence is a consequence of present magnetic resonance imaging resolutions having reached less than $(100\text{ nm})^3$, a size scale at which statistical spin fluctuations begin to dominate the polarization dynamics. Here, we demonstrate a technique that creates spin order in nanometre-scale ensembles of nuclear spins by harnessing these fluctuations to produce polarizations both larger and narrower than the thermal distribution. This method may provide a route to enhancing the weak magnetic signals produced by nanometre-scale volumes of nuclear spins or a way of initializing the nuclear hyperfine field of electron-spin qubits in the solid state.

Spin noise is a phenomenon present in all spin ensembles that begins to exceed the mean thermal polarization as the size of the ensemble shrinks. These fluctuations have a random amplitude and phase and have been observed in a wide variety of nuclear spin systems including in liquids by conventional nuclear magnetic resonance^{7,8} (NMR) and in the solid state using a superconducting quantum interference device², by force-detected magnetic resonance⁹ or by nitrogen–vacancy magnetometry^{4,5}. In addition to finding applications in nanometre-scale magnetic resonance imaging (MRI), spin noise has been used in MRI specially adapted for the investigation of extremely delicate specimens, in which external radiofrequency irradiation is not desired¹⁰. Through the hyperfine interaction, nuclear spin noise also sets limits on the coherence of electron spin qubits in the solid state^{11–15}. Various efforts to mitigate these nuclear field fluctuations by hyperfine-mediated nuclear state preparation have been developed, both in quantum dots^{16–20} and in nitrogen–vacancy centres in diamond²¹. We report on a manipulation and initialization technique that applies to arbitrary nanometre-scale samples; that is, it does not require specialized structures providing a controllable electronic spin and a strong hyperfine interaction. Rather, our technique requires a detector sensitive enough to resolve nuclear spin noise and the ability to apply radiofrequency electromagnetic pulses.

Conventional NMR and MRI techniques rely on manipulating the mean thermal polarization to produce signals. Statistical nuclear polarization fluctuations exceed the mean thermal polarization below a critical number of spins $N_c = 3/(I(I+1))(k_B T/\hbar\gamma B_0)^2$, where I is the spin quantum number, k_B is the Boltzmann constant, T is the temperature, γ is the gyromagnetic ratio and B_0 is

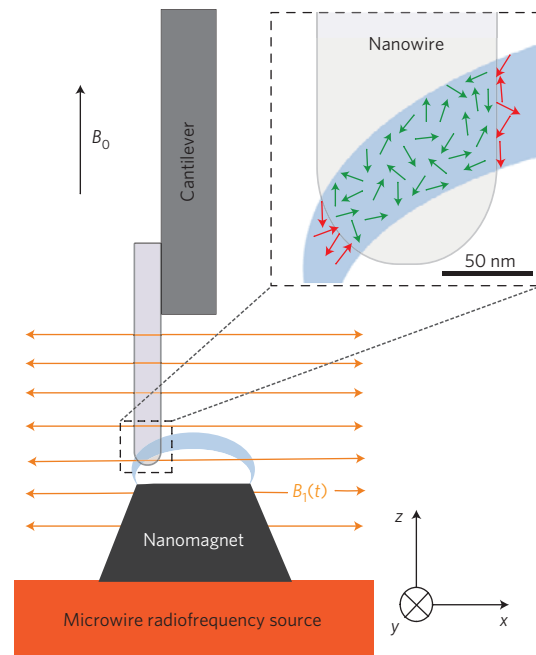


Figure 1 | Schematic of the experimental geometry. The end of the nanowire, which is affixed to an ultrasensitive cantilever, is positioned 100 nm away from the nanomagnet. Below the nanomagnet, a microwire radiofrequency source generates ARP pulses to invert the nuclear spin ensemble within a nanometre-scale resonant slice (in light blue). Two types of spin ensemble are investigated: one composed of ^{31}P nuclei within the nanowire lattice (green spins) and another consisting of ^1H nuclei from the thin adsorbate layer on the nanowire surface (red spins).

the magnetic field²². For ^1H spins at $T = 1\text{ K}$ in an applied magnetic field $B_0 = 1\text{ T}$, $N_c = 10^6$, which in most organic samples corresponds to a critical volume $V_c = (24\text{ nm})^3$. Under the ambient conditions of recent NMR experiments with nitrogen–vacancy spin sensors, statistical polarization begins to dominate for even larger samples with $V_c = (6\text{ }\mu\text{m})^3$ (refs 4,5). To measure and initialize such ensembles, it is therefore worthwhile to consider techniques designed to both detect and control nuclear polarization fluctuations. Although nuclear magnetic signals from such small volumes are weak, if a detector is able to resolve spin noise in real time, that is, faster than the spin correlation time τ_m , large fluctuations can be captured. Once captured, these fluctuations

¹Department of Physics, University of Basel, 4056 Basel, Switzerland, ²Department of Applied Physics, Eindhoven University of Technology, 5600 MB Eindhoven, The Netherlands, ³Kavli Institute of Nanoscience, Delft University of Technology, 2600 GA Delft, The Netherlands.

*e-mail: martino.poggio@unibas.ch

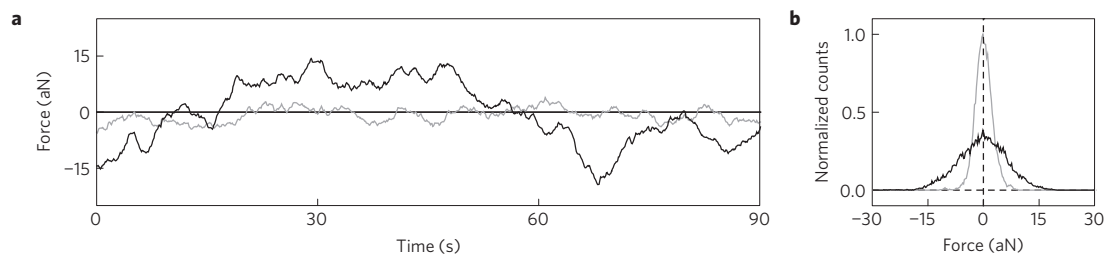


Figure 2 | Spin noise from an ensemble of $6 \times 10^5 < N < 1 \times 10^7$ ^{31}P spins in an InP nanowire. **a**, In-phase $X(t)$ (black) and quadrature $Y(t)$ (grey) force on the cantilever demodulated at the cantilever frequency. $T = 4.2$ K and $B_{\text{ext}} = 6$ T. The lock-in time constant is set to $\tau_l = 5$ s, to match the correlation time $\tau_m = 3.6$ s of the spin fluctuations and to reject the cantilever's thermal fluctuations with a correlation time $\tau_c = 65$ ms. The thermal noise $Y(t)$ sets the limit for the MRFM detection sensitivity at a polarization equivalent to ~ 250 ^{31}P nuclear spins r.m.s. **b**, Histograms of $X(t)$ and $Y(t)$ recorded for 1 h. Gaussian fits to these histograms give $\sigma_X = 6.4$ aN and $\sigma_Y = 2.1$ aN.

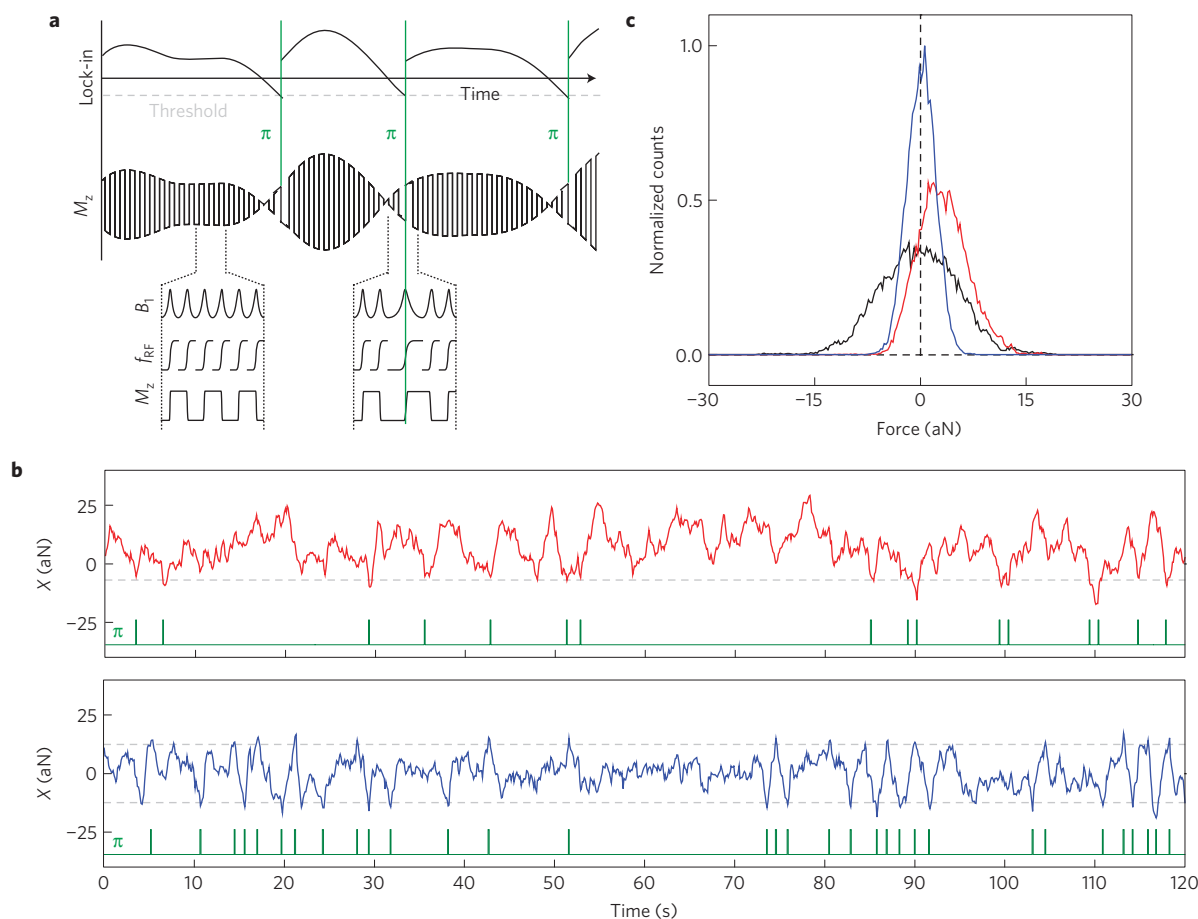


Figure 3 | Rectifying and narrowing the nuclear spin polarizations. **a**, Schematic describing the conditional application of π -inversion pulses. **b**, $X(t)$ recorded with a rectification threshold of -5 aN (red) and with an absolute value threshold of 12.5 aN (blue). Green pulses show the times at which π -inversions are applied. $\tau_l = 0.8$ s in both cases. The sample is an ensemble of $6 \times 10^5 < N < 1 \times 10^7$ ^{31}P spins in an InP nanowire at $T = 4.2$ K and $B_{\text{ext}} = 6$ T. **c**, Histograms of $X(t)$ recorded over 1 h corresponding to the natural (black), rectified (red) and narrowed (blue) cases. The mean polarization of the rectified distribution is 2.9 aN, compared with 0.0 aN of the natural distribution. The standard deviation of the narrowed distribution is 2.0 aN, compared with 5.6 aN of the natural distribution.

can then be used to initialize the polarization of nanometre-scale spin ensembles with a fixed sign and magnitude. Such initialization schemes could provide the basis for enhancing signals from small samples and for realizing advanced pulse protocols that can be borrowed directly from conventional NMR.

In 2005, a technique for the capture and storage of electron spin fluctuations was demonstrated²³. Inspired by this work, we have adapted the protocol to nanometre-scale ensembles of nuclear spins. Given the relevance of these ensembles to

nanometre-scale MRI and to the decoherence of solid-state qubits, this implementation could find wide applicability. Furthermore, the longer spin relaxation time of nuclear spins compared with electron spins—sometimes as long as several hours at cryogenic temperatures—allows captured spin order to be stored for far longer times.

We study two separate samples: an InP and a GaP nanowire. Using a magnetic resonance force microscope (MRFM) shown schematically in Fig. 1, we measure the polarization of nanometre-

scale ensembles of ^{31}P nuclei within each nanowire and of ^1H nuclei contained in the hydrocarbon adsorbate layer on the surface. Adiabatic rapid passage (ARP) pulses of the transverse field²⁴ are used to cyclically invert the polarization of nanometre-scale volumes of a particular nuclear isotope. In a magnetic field gradient, these periodic inversions generate an alternating force that drives the mechanical resonance of an ultrasensitive cantilever.

We feed the cantilever force signal to a lock-in amplifier referenced to the periodic spin inversions and monitor its in-phase (X) and quadrature (Y) amplitudes. The limiting source of noise in the measurement is the thermal force acting on the cantilever, which has a random phase and on average contributes equally to X and Y . On the other hand, force fluctuations due to the nuclear spin polarization are in phase with the inversion pulses and contribute only to X . Thus, as shown in Fig. 2a, we can monitor $Y(t)$, the thermal force, and $X(t)$, the thermal force plus the force due to the nuclear spin inversions. $X(t)$ is dominated by the large fluctuations and the long τ_m of the spin noise, whereas the thermal noise in $Y(t)$ has a smaller amplitude and a shorter correlation time set by the damped cantilever force sensor. τ_m is limited by the magneto-mechanical noise originating from the thermal motion of the cantilever in a magnetic field gradient and by the ARP pulse parameters²⁵. As the contribution of the spin signal to $X(t)$ is large enough, we can follow—in real time—the instantaneous nuclear spin imbalance in the rotating frame. Figure 2b shows the variances σ_X^2 and σ_Y^2 , which give the variance due only to the thermal noise $\sigma_T^2 = \sigma_Y^2$ and the variance due only to the spin noise, $\sigma_S^2 = \sigma_X^2 - \sigma_T^2$.

The real-time measurement of spin noise allows us to react to and control the fluctuations in polarization²³. As a demonstration, we conditionally apply radiofrequency π -inversion pulses to both rectify and narrow the naturally occurring polarization distribution. As shown in Fig. 3, when $X(t)$ exceeds a predetermined threshold, the protocol applies a π -inversion. In this way, we can either rectify or narrow $X(t)$ by setting appropriate thresholds, resulting in both hyperpolarized and narrowed nuclear spin distributions in the rotating frame. The same concept of applying feedback to real-time measurements was applied in ref. 20 to fluctuations in the nuclear hyperfine field in a gate-defined double quantum dot. In that case, suppressed nuclear spin fluctuations were shown to enhance the electron spin qubit dephasing time nearly tenfold.

In addition to controlling an ensemble's natural spin fluctuations, we can also capture especially large fluctuations²³. As shown in Fig. 4, we continuously measure the rotating-frame spin fluctuations by monitoring $X(t)$. Once $X(t)$ reaches a predetermined threshold X_c , the ARP pulses are tuned out of resonance with the nuclear spin ensemble, leaving the instantaneous spin polarization pointing along the total static magnetic field \mathbf{B}_0 and transferring the transient spin order to the laboratory frame. As the spin ensemble does not respond to the off-resonant ARP pulses, the cantilever is no longer driven by spin forces. In this way, hyperpolarized states of a desired orientation along \mathbf{B}_0 can be captured and stored in the laboratory frame for as long as the spin-lattice relaxation time T_1 . To confirm that the nuclear polarization has in fact been stored, we can reapply the resonant ARP pulses after some storage time T_{store} to readout the polarization. Once again, spin inversions drive the cantilever motion and the amplitude of $X(t)$ reflects the size of the retrieved fluctuation.

In an idealized case, in which the spin component of the captured fluctuation X_c is fully projected onto \mathbf{B}_0 , the stored fluctuation X_s will be normally distributed with a mean $\langle X_s \rangle = (X_c \sigma_S^2) / (\sigma_S^2 + \sigma_T^2)$ and a variance $\sigma_{X_s}^2 = (\sigma_S^2 \sigma_T^2) / (\sigma_S^2 + \sigma_T^2)$ (Supplementary Information). The fact that $\langle X_s \rangle < X_c$ reflects the finite signal to noise ratio (SNR) of the measurement, in this case limited by the cantilever's thermal noise. Note also that the distribution of the stored polarization is narrowed; that is, it has a reduced variance, compared with the variance of spin fluctuations under normal evolution ($\sigma_{X_s}^2 < \sigma_S^2$).

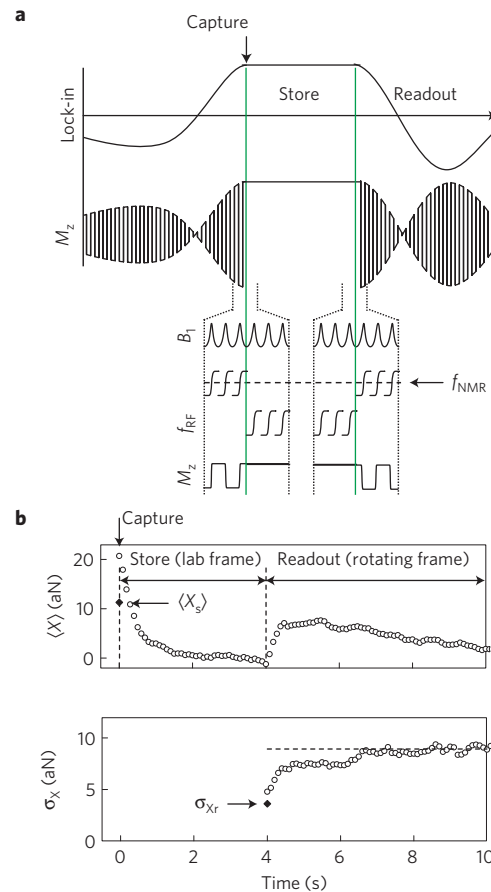


Figure 4 | Capture-store-readout pulse sequence. **a**, Schematic diagram describing the capture-store-readout pulse sequence. **b**, Top: $\langle X(t) \rangle$ averaged over 100 capture-store-readout sequences showing $T_{\text{store}} = 4$ s for a ^{31}P spin ensemble with $6 \times 10^5 < N < 1 \times 10^7$ in a GaP nanowire. The mean stored fluctuation $\langle X_s \rangle$ is shown as a filled diamond. $T = 4.2$ K and $B_{\text{ext}} = 6$ T. The signal's decay after the capture is due to the lock-in time constant $\tau_l = 0.4$ s. The readout fluctuations decay over a time $\tau_m = 3.8$ s. Bottom: $\sigma_X(t)$ taken over the same 100 sequences showing the narrowed standard deviation of the retrieved fluctuation σ_{X_r} (filled diamond) as it equilibrates back to its rotating frame value (dashed line). Note that τ_l is much shorter than the time over which $\sigma_X(t)$ evolves, excluding the lock-in as a source of the behaviour.

In the limit of large SNR ($\sigma_S^2 \gg \sigma_T^2$), $\langle X_s \rangle \rightarrow X_c$ and $\sigma_{X_s}^2 \rightarrow 0$. If during T_{store} this stored polarization undergoes negligible relaxation in the laboratory frame, the corresponding retrieved fluctuation X_r has a mean $\langle X_r \rangle = \langle X_s \rangle$ and a variance $\sigma_{X_r}^2 = \sigma_{X_s}^2 + \sigma_T^2 < \sigma_X^2$. Note that $\sigma_{X_r}^2 > \sigma_{X_s}^2$ owing to the finite SNR of the retrieval measurement.

To compare our experiments to this idealized case, we measure $\langle X_r \rangle$ and $\sigma_{X_r}^2$ for nanometre-scale ^{31}P and ^1H spin ensembles. As shown in Fig. 5, $\langle X_r \rangle$ and τ_m are extracted from bi-exponential fits to $\langle X(t) \rangle$ during the readout sequence using our knowledge of the lock-in time constant τ_l . Deviations of $\langle X_r \rangle$ from $\langle X_s \rangle$ could be caused by the spin-lattice relaxation in the laboratory frame—set by T_1 —or by the incomplete projection of the polarization onto \mathbf{B}_0 . For both ^{31}P and ^1H in Fig. 5a,b, these deviations are negligible within our error. Figure 4b shows the reduced variance of the retrieved polarization $\sigma_{X_r}^2$, eventually approaching the variance under normal evolution after a time of the order of τ_m in the rotating frame. This result demonstrates that the distribution of the captured fluctuations is indeed narrowed relative to the natural distribution of the nuclear spin fluctuations. The ability to prepare such distributions may find application in quantum information

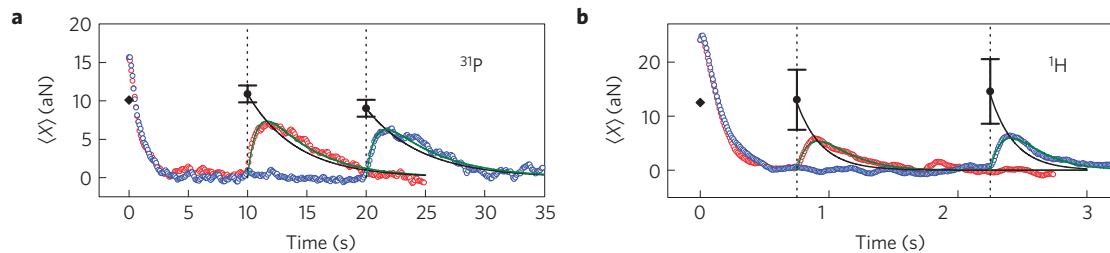


Figure 5 | Storage of spin order in the laboratory frame. **a**, Two capture-store-readout sequences for different T_{store} for an ensemble of $6 \times 10^5 < N < 1 \times 10^7$ ^{31}P spins in an InP nanowire. Fits to $\langle X(t) \rangle$ during the readout take into account the lock-in time constant $\tau_l = 0.8$ s (green lines) and allow us to recover the value of the retrieved fluctuation $\langle X_r \rangle$ (filled circles) and its exponential decay with $\tau_m = 4.3$ s without the effect of τ_l (black lines). Error bars are set by the 95% confidence interval of the extracted fit parameter. The filled diamond indicates the mean stored fluctuation $\langle X_s \rangle$. **b**, The same measurement done for $2 \times 10^5 < N < 7 \times 10^5$ ^1H spins on a GaP nanowire with $\tau_l = 140$ ms, where τ_m is found to be 190 ms. Again $\langle X_r \rangle$ are shown as filled circles and $\langle X_s \rangle$ as a filled diamond. Limitations of the experimental hardware prevented measurements for larger T_{store} , although our data show that $T_1 \gg 20$ s for ^{31}P in InP and $T_1 \gg 2.5$ s for ^1H on GaP. In both cases $T = 4.2$ K and $B_{\text{ext}} = 6$ T.

processing with solid-state electron spins, which is often limited by the random nuclear field distribution in the host material^{16–20}. The nuclear spin ensemble in such a system could be initialized before each measurement by a scheme based on the capture of random polarization fluctuations, thus enhancing the electron spin dephasing time. The degree of narrowing demonstrated in Fig. 4b represents a factor of 2.5 reduction in standard deviation compared with the natural distribution and is limited by the SNR of the measurement.

The size of the captured spin fluctuation is, in principle, limited only by the amount of time one is willing to wait. For the normally distributed random variable $X(t)$, the average amount of wait time required to capture a fluctuation X_c is given by $T_{\text{wait}} = (2/n_0)e^{X_c^2/(2\sigma_X^2)}$, where n_0 is the average number of times $X(t)$ crosses zero per second²⁶ (Supplementary Information). For example, given that $n_0 = 0.2$ Hz is a typical value in our experiments, fluctuations of $3\sigma_X$ are expected after just $T_{\text{wait}} = 15$ min, or alternatively for $T_{\text{wait}} = 1$ h, a fluctuation of $3.4\sigma_X$ is expected. For a ^{31}P spin ensemble with $N = 10^6$ at $B_0 = 6$ T and $T = 4.2$ K, the standard deviation of the statistical polarization fluctuations is given by $\rho_S = \sqrt{((I+1)/3I)(1/N)} = 0.1\%$ and its mean thermal polarization is $\rho_B = ((I+1)/3)((\hbar\gamma B_0)/k_B T) = 0.06\%$ (ref. 22). Therefore, in the limit of large SNR where σ_X is dominated by spin fluctuations, we can expect to capture polarizations of $5.1\rho_B$ in 15 min and $5.8\rho_B$ in 1 h. The polarization captured in a given T_{wait} could be increased even further by reducing τ_m and therefore increasing n_0 , for example, through the periodic randomization of the spin ensemble using bursts of $\pi/2$ -pulses²⁷. In principle, the nuclear spin decoherence time T_2 sets the lower limit for τ_m . As the size of the spin ensemble shrinks, the size of the achievable polarization increases as $1/\sqrt{N}$, making such a protocol increasingly relevant as detection volumes continue to shrink. Given that conventional pulse protocols based on thermal polarization require an initialization step taking at least T_1 , waiting for an extended time to capture a large spin fluctuation may be attractive—especially when the magnitude of the captured fluctuation greatly exceeds the possible thermal polarization. Nevertheless, given the exponential time required, this method cannot compete with standard hyperpolarization techniques when they are possible.

Note that the crucial step in the capture protocol is that the monitoring and capture occurs in the rotating frame, where the time between statistically independent spin polarizations—set by τ_m —is much faster than the equivalent time T_1 in the laboratory frame (Supplementary Information). We assume that the spin relaxation characterized by τ_m produces random and statistically independent spin polarizations. This assumption is supported by both the measurement of a Gaussian distribution in Fig. 2b and by the exponentially decaying autocorrelation function measured in ref. 27 for similar spin fluctuations. This short rotating-frame

correlation time allows the system to quickly explore its spin configuration space. On the other hand, once a large fluctuation is captured and transferred to the laboratory frame, the long T_1 effectively freezes the ensemble in this rare configuration.

We therefore show the capture and storage of large polarization fluctuations arising from spin noise in nanometre-scale nuclear spin ensembles with $N \sim 10^6$. The ability to prepare a small nuclear spin ensemble into a polarized and narrowed distribution is important for the development of future nanometre-scale NMR techniques or possibly for the implementation of solid-state spin qubits. Although these results were obtained with a low-temperature MRFM, the capture and storage of spin fluctuations should be generally applicable to any technique capable of detecting and addressing nanometre-scale volumes of nuclear spins in real time. When polarization cannot be created through standard hyperpolarization techniques such as dynamic nuclear polarization, this method provides a viable alternative. The ensembles polarized in this work, nanometre-scale volumes of ^1H on an adsorbate layer and ^{31}P in a single semiconducting nanowire, demonstrate the types of sample that could benefit from this technique. One could imagine, for instance, such nuclear polarization capture processes enhancing the weak MRI signals of a nanometre-scale ^1H -containing biological sample or of a semiconducting nanostructure.

Methods

The MRFM consists of a nanomagnetic tip integrated on top of a microwave radiofrequency source, an ultrasensitive Si cantilever and a fibre-optic interferometer to measure its displacement²⁸. The entire apparatus operates in vacuum better than 10^{-6} mbar, at temperatures down to $T = 4.2$ K and in an applied longitudinal field up to $B_{\text{ext}} = 6$ T. The nanowire of interest is attached to the end of the cantilever and is positioned within 100 nm of the nanomagnetic tip, as shown schematically in Fig. 1. Here the field produced by the tip, \mathbf{B}_{tip} , results in $\mathbf{B}_0 = \mathbf{B}_{\text{ext}} + \mathbf{B}_{\text{tip}}$, whereas the microwire produces a transverse radiofrequency field $\mathbf{B}_1(t)$. ARP pulses invert the nuclear spin polarization because the polarization follows (or is spin-locked to) the time-dependent effective field $\mathbf{B}_{\text{eff}}(t) = (B_0 - 2\pi f_{\text{RF}}(t)/\gamma)\mathbf{e}_z + (1/2)B_1(t)\mathbf{e}_x$ in a frame rotating with the radiofrequency field, where $f_{\text{RF}}(t)$ is the instantaneous frequency of the ARP pulses, $B_1(t)$ their amplitude, and the unit vectors are defined in the rotating frame.

The volume of inverted spins, known as the resonant slice, is determined by the spatial dependence of \mathbf{B}_{tip} and the parameters of the pulses. The number of nuclear spins in this volume is in turn related to the measured force variance by the approximation $\sigma_s^2 \approx N(I(I+1)/3)(\hbar\gamma)^2(\partial B_0/\partial x)^2$, where \mathbf{e}_x is the direction of cantilever oscillation²². This relation holds as long as the volume of spins is small enough that the gradient $\partial B_0/\partial x$ is nearly constant throughout; otherwise it provides a lower bound N_{lower} on the number of spins. From measurements of the magnetic field gradient in the vicinity of the tip, we estimate that $\partial B_0/\partial x = 1.5 \times 10^6$ T m⁻¹ at the position of the detection volume. To set an upper bound for the number of spins N_{upper} , we make a model of the magnetic field profile produced by the nanomagnetic tip and numerically integrate the spatially dependent gradient over the sample volume contained in the resonant slice (Supplementary Information). The typical size of the spin ensembles we measure is between 2×10^5 and 7×10^5 for ^1H and between 6×10^5 and 1×10^7 for

³¹P. Given the density of typical adsorbate layers and InP and GaP, the detection volumes discussed here are between $(13 \text{ nm})^3$ and $(21 \text{ nm})^3$ for ¹H and between $(30 \text{ nm})^3$ and $(80 \text{ nm})^3$ for ³¹P.

Ultrasensitive cantilevers are made from undoped single-crystal Si and measure 120 μm in length, 4 μm in width and 0.1 μm in thickness. In vacuum and at the operating temperatures, the nanowire-loaded cantilevers have resonant frequencies $f_c = 2.4$ and 3.5 kHz, intrinsic quality factors $Q_0 = 3.0 \times 10^4$ and 3.5×10^4 , and spring constants $k = 60$ and 100 $\mu\text{N m}^{-1}$ for the InP and GaP nanowire experiments respectively. Both nanowires are grown with the vapour–liquid–solid method in a metal-organic vapour-phase epitaxy reactor using gold droplets as catalyst²⁹. The InP nanowire is 8 μm long; its diameter shrinks from 200 nm to 60 nm along its length; and it is tipped by a 60-nm-diameter Au catalyst particle, left over from the growth process. The GaP nanowire is 10 μm long; its diameter is 1.0 μm ; and it has a 1.5- μm -long tapered tip that reaches 90 nm in diameter at the Au droplet. In this case we remove the Au droplet by cutting off the end of the nanowire with a focused ion beam, resulting in a 300-nm-diameter GaP tip. Finally, we sputter a 5 nm layer of Pt onto the nanowire to shield electrostatic interactions. Each nanowire is affixed to the end of the cantilever with less than 100 fl of epoxy (Gatan G1). In the attachment process, we employ an optical microscope equipped with a long working distance and a pair of micromanipulators. During the measurement, the cantilever is actively damped to give it a fast response time of $\tau_c = 65$ ms. Up to 50 nW of laser light at 1,550 nm are incident on the cantilever as part of the fibre-optic interferometer. The nanomagnetic tips are truncated cones of Dy fabricated by optical lithography³⁰. For the InP (GaP) nanowire experiment the tip measures 225 (280) nm in height, 270 (250) nm in upper diameter, and 380 (500) nm in lower diameter. The radiofrequency source, on which the Dy tip sits, is a 2- μm -long, 1- μm -wide and 200-nm-thick Au microwire. By positioning each nanowire within 100 nm of the combined structure, the detection volume can be exposed to spatial magnetic field gradients exceeding $1.5 \times 10^6 \text{ T m}^{-1}$ and radiofrequency $B_1(t)$ fields larger than 20 mT without significant changes in the experimental operating temperature. We use hyperbolic secant ARP pulses with $\beta = 10$ and a modulation amplitude set to 500 kHz peak-to-peak for ³¹P and 1 MHz for ¹H (ref. 24). These parameters, combined with the geometry of the sample and the profile of $\partial B_0/\partial x$, determine the size of the detection volume.

Received 1 April 2013; accepted 21 July 2013; published online 25 August 2013

References

- Bloch, F. Nuclear induction. *Phys. Rev.* **70**, 460–474 (1946).
- Sleator, T., Hahn, E. L., Hilbert, C. & Clarke, J. Nuclear-spin noise. *Phys. Rev. Lett.* **55**, 1742–1745 (1985).
- Degen, C. L., Poggio, M., Mamin, H. J., Rettner, C. T. & Rugar, D. Nanoscale magnetic resonance imaging. *Proc. Natl Acad. Sci. USA* **106**, 1313–1317 (2009).
- Mamin, H. J. *et al.* Nanoscale nuclear magnetic resonance with a nitrogen-vacancy spin sensor. *Science* **339**, 557–560 (2013).
- Staudacher, T. *et al.* Nuclear magnetic resonance spectroscopy on a (5-nanometer)³ sample volume. *Science* **339**, 561–563 (2013).
- Nichol, J. M., Naibert, T. R., Hemesath, E. R., Lauhon, L. J. & Budakian, R. Nanoscale Fourier-transform MRI of spin noise. Preprint at <http://arxiv.org/abs/1302.2977> (2013).
- McCoy, M. A. & Ernst, R. R. Nuclear spin noise at room temperature. *Chem. Phys. Lett.* **159**, 587–593 (1989).
- Guéron, M. & Leroy, J. L. NMR of water protons. The detection of their nuclear-spin noise, and a simple determination of absolute probe sensitivity based on radiation damping. *J. Magn. Reson.* **85**, 209–215 (1989).
- Mamin, H. J., Budakian, R., Chui, B. W. & Rugar, D. Magnetic resonance force microscopy of nuclear spins: detection and manipulation of statistical polarization. *Phys. Rev. B* **72**, 024413 (2005).
- Müller, N. & Jerschow, A. Nuclear spin noise imaging. *Proc. Natl Acad. Sci. USA* **103**, 6790–6792 (2006).
- Merkulov, I. A., Efros, A. I. L. & Rosen, M. Electron spin relaxation by nuclei in semiconductor quantum dots. *Phys. Rev. B* **65**, 205309 (2002).
- Khaetskii, A. V., Loss, D. & Glazman, L. Electron spin decoherence in quantum dots due to interaction with nuclei. *Phys. Rev. Lett.* **88**, 186802 (2002).
- Childress, L. *et al.* Coherent dynamics of coupled electron and nuclear spin qubits in diamond. *Science* **314**, 281–285 (2006).
- Kuhlmann, A. V. *et al.* Charge noise and spin noise in a semiconductor quantum device. *Nature Phys.* <http://dx.doi.org/10.1038/nphys2688> (2013).
- Chekhovich, E. A. *et al.* Nuclear spin effects in semiconductor quantum dots. *Nature Mater.* **12**, 494 (2013).
- Coish, W. A. & Loss, D. Hyperfine interaction in a quantum dot: Non-Markovian electron spin dynamics. *Phys. Rev. B* **70**, 195340 (2004).
- Reilly, D. J. *et al.* Suppressing spin qubit dephasing by nuclear state preparation. *Science* **321**, 817–821 (2008).
- Latta, C. *et al.* Confluence of resonant laser excitation and bidirectional quantum-dot nuclear-spin polarization. *Nature Phys.* **5**, 758–763 (2009).
- Vink, I. *et al.* Locking electron spins into magnetic resonance by electron-nuclear feedback. *Nature Phys.* **5**, 764–768 (2009).
- Bluhm, H., Foletti, S., Mahalu, D., Umansky, V. & Yacoby, A. Enhancing the coherence of a spin qubit by operating it as a feedback loop that controls its nuclear spin bath. *Phys. Rev. Lett.* **105**, 216803 (2010).
- Togan, E., Chu, Y., Imamoglu, A. & Lukin, M. D. Laser cooling and real-time measurement of the nuclear spin environment of a solid-state qubit. *Nature* **478**, 497–501 (2011).
- Xue, F., Weber, D. P., Peddibhotla, P. & Poggio, M. Measurement of statistical nuclear spin polarization in a nanoscale GaAs sample. *Phys. Rev. B* **84**, 205328 (2011).
- Budakian, R., Mamin, H. J., Chui, B. W. & Rugar, D. Creating order from random fluctuations in small spin ensembles. *Science* **307**, 408–411 (2005).
- Tannús, A. & Garwood, M. Improved performance of frequency-swept pulses using offset-independent adiabaticity. *J. Magn. Reson. A* **120**, 133–137 (1996).
- Degen, C. L., Poggio, M., Mamin, H. J. & Rugar, D. Nuclear spin relaxation induced by a mechanical resonator. *Phys. Rev. Lett.* **100**, 137601 (2008).
- Rice, S. O. Mathematical analysis of random noise. *AT&T Tech. J.* **24**, 46–156 (1945).
- Degen, C. L., Poggio, M., Mamin, H. J. & Rugar, D. Role of spin noise in the detection of nanoscale ensembles of nuclear spins. *Phys. Rev. Lett.* **99**, 250601 (2007).
- Poggio, M., Degen, C. L., Rettner, C. T., Mamin, H. J. & Rugar, D. Nuclear magnetic resonance force microscopy with a microwire rf source. *Appl. Phys. Lett.* **90**, 263111 (2007).
- Assali, S. *et al.* Direct band gap wurtzite gallium phosphide nanowires. *Nano Lett.* **13**, 1559–1563 (2013).
- Mamin, H. J., Rettner, C. T., Sherwood, M. H., Gao, L. & Rugar, D. High field-gradient dysprosium tips for magnetic resonance force microscopy. *Appl. Phys. Lett.* **100**, 013102 (2012).

Acknowledgements

The authors thank C. L. Degen, C. Klöffel, T. Poggio and R. J. Warburton for illuminating discussions; H. S. Solanki for experimental assistance; and S. Keerthana for assistance with a figure. We acknowledge support from the Canton Aargau, the Swiss National Science Foundation (SNF, Grant No. 200020-140478), the Swiss Nanoscience Institute, and the National Center of Competence in Research for Quantum Science and Technology.

Author contributions

P.P. and M.P. conceived and designed the experiments in collaboration with F.X. P.P. carried out the experiments, to which F.X. made early contributions. P.P. and M.P. analysed the data and wrote the manuscript. P.P. and F.X. prepared the samples and devices. The nanowires were grown by H.I.T.H., S.A. and E.P.A.M.B. All authors discussed the results and contributed to the manuscript.

Additional information

Supplementary information is available in the [online version of the paper](#). Reprints and permissions information is available online at www.nature.com/reprints. Correspondence and requests for materials should be addressed to M.P.

Competing financial interests

The authors declare no competing financial interests.